Ureteral morphology and pathology during urolithiasis in cats

Osamu Ichii[1,2*], Kazuhisa Oyamada[3], Hazuki Mizukawa[4], Nozomu Yokoyama[5], Takashi Namba[1], Yuki Otani[1,2], Noboru Sasaki[6], Teppei Nakamura[1,7], Yaser Hosny Ali Elewa[1,8], and Yasuhiro Kon[1]

[1]Laboratory of Anatomy, Department of Basic Veterinary Sciences, Faculty of Veterinary Medicine, Hokkaido University, Sapporo, Japan

[2]Laboratory of Agrobiomedical Science, Faculty of Agriculture, Hokkaido University, Sapporo, Japan

[3]Matsubara Animal Hospital, Matsubara, Japan

[4]Department of Science and Technology for Biological Resources and Environment, Graduate School of Agriculture, Ehime University, Japan.

[5]Veterinary Teaching Hospital, Graduate School of Veterinary Medicine, Hokkaido University, Japan.

[6]Laboratory of Veterinary Internal Medicine, Department of Veterinary Clinical Sciences, Faculty of Veterinary Medicine, Hokkaido University, Sapporo, Japan

[7]Department of Biological Safety Research, Chitose Laboratory, Japan Food Research Laboratories, Chitose, Japan

[8]Department of Histology, Faculty of Veterinary Medicine, Zagazig University, Zagazig, Egypt

*Corresponding author: Osamu Ichii, DVM, PhD

Laboratory of Anatomy, Department of Basic Veterinary Sciences, Faculty of Veterinary Medicine, Hokkaido University, Kita 18, Nishi 9, Kita-ku, Sapporo 060-0818, Japan

E-mail: ichi-o@vetmed.hokudai.ac.jp

Tel./Fax: +81-11-706-5188

Abstract

Cats show high susceptibility to the urinary organ-related diseases. This study investigated the morphological characteristics of healthy ureters and compared them with surgically resected ureters distal to the lesion obstructed by urolithiasis in cats. Healthy ureters (total length 9.88 ± 0.38 cm) developed adventitia composed of collagen fibers (ADCF), containing longitudinal muscular layer, toward the distal segment. Healthy ureter was smallest in the middle segment (4.71–6.90 cm from the urinary bladder) with significantly decreased area of its lumen and submucosa from the proximal segment. Diseased cats showed a high incidence of calcium oxalate (CaOx) urolithiasis with renal dysfunction, regardless of age, sex, and body size. Their ureters showed increased perimeters, inflammation, and decreased nerves in ADCF. Collagen fibers were increased in the submucosal area, intermuscular spaces, and ADCF, especially near the obstructed lesion. The mean resected ureter length was 5.66 ± 0.49 cm, suggesting a high obstruction risk in the middle segment. The middle segment also increased the cross area of ureter and ADCF, regardless of the distance from the obstructed lesion. Importantly, the ureters of several cases showed a lack of transitional epithelium or its hyperplasia, and some of them formed the mucosal folds. Thus, we report the characteristics and histopathological features of cat ureters; especially, the decreases of ureter size, lumen area, and submucosa area from proximal to middle segment in healthy and ADCF alternations in urolithiasis, including increased connective tissues with inflammation and decreased nerves, would be crucial to consider the pathogenesis of feline ureteral obstruction.

Running head: Cat ureter and urolithiasis

Keywords: Cat, ureter, histology, histopathology, calcium oxalate, urolithiasis

Highlights

- HC ureter was smallest in the middle segment (4.7–6.9 cm from the urinary bladder)
- Ureter with feline urolithiasis (UWFU) showed increased perimeters and inflammation
- UWFU decreased nerves in adventitia composed of collagen fibers
- Histological data suggested the high obstruction risk in the middle segment of UWFU

Introduction

In small animal veterinary medicine, large survey data reported that approximately 4% of dogs and 12% of cats die from a renal disorder in UK (Lewis et al., 2018; O'Neill et al., 2015). In particular, data from Europe and the USA indicated that 4.6% of cats in private practices, and 7% to 8% of those in veterinary teaching hospitals show feline lower urinary tract disease (FLUTD), manifesting as pollakiuria, hematuria, stranguria, or complete or incomplete urinary tract obstruction (Dru Forrester and Roudebush, 2007). FLUTD cases with urinary tract obstruction can be cause uremia and hyperkalemia, the mortality of which reaches 5% (Kaul et al., 2020). FLUTD is caused by bacterial infections, urethral plugs, anatomical defects, neoplasia, idiopathic cystitis, and urolithiasis (Dru Forrester and Roudebush, 2007; Kaul et al., 2020; Lulich et al., 2016).

In a German cat population, urolithiasis is observed in 7.0% of animals with FLUTDs (n = 302) (Dorsch et al., 2014). The main components of urinary calculus are calcium oxalate (CaOx) or struvite in dogs and cats. In cats, a Canadian study reported that 49% or 43% of bladder uroliths were composed of struvite or calcium oxalate, respectively (Houston and Moore, 2009). In particular, feline urolithiasis caused by CaOx is increasing due to the aging of individuals and promotion of urine acidification or animal protein-containing diets (Lulich et al., 2016; Osborne et al., 2009). Hypercalcemia caused by primary hyperparathyroidism or feline idiopathic hypercalcemia is another known risk factor for CaOx urolithiasis (Finch, 2016; Lulich et al., 2016). CaOx is insoluble, and it is important to prevent its formation; to this end, potassium citrate and thiazide diuretics have been used for therapeutic purposes (Lulich et al., 2016; Osborne et al., 2009). CaOx obstructing the lower urinary tract, including the urinary bladder or urethra, can be eliminated by minimally invasive procedures such as lithotripsy or basket retrieval (Lulich et al., 2016). However, the upper urinary tract, including the renal pelvis or ureters, should be immediately eliminated by surgical procedures, such as stents, bypasses, ureterotomy, and resection and anastomosis, because it can cause serious symptoms or irreversible morpho-functional alternation of kidneys and ureters, ultimately leading to hydronephrosis or hydroureter (Berent et al., 2018; Lulich et al., 2016).

The elucidation of species-specific morphological features in each organ would improve the understanding of the relationship between anatomy, physiology, and pathology. Given that cats show high susceptibility to urinary tract diseases, including urolithiasis, the clarification of their

pathology is crucial in the field of veterinary medicine. Almost all previous studies have mainly focused on the pathological effects of diet or animal health status, such as infection, endocrinopathy, and congenital urinary tract disorders, as risk factors for cat urolithiasis (Brourman, 2011; Dru Forrester and Roudebush, 2007; Houston and Moore, 2009; Kaul et al., 2020; Lulich et al., 2016; Nesser et al., 2018; Osborne et al., 2009, 1979). However, the normal histological structures and pathological alternations of cat ureters have not been fully investigated.

In this study, we examined the normal histological features of cat ureters in several compartments. Moreover, the histopathological changes due to urolithiasis were examined in surgically resected ureters. Our results provide a crucial basis for understanding the anatomical and physiological characteristics, as well as the pathogenesis of cat ureters.

Materials and Methods

Sample preparations from healthy cats

The age and body weight (BW) of the animals were recorded before sampling. We obtained the ureters from healthy cats (*n* = 4 animals, 8 ureters, 1.08 ± 0.04 years), which were euthanized for use in other experiments approved by the Institutional Animal Care and Use Committee of the Faculty of Veterinary Medicine, Hokkaido University (approval no. 14-0054, 20-0081). The obtained ureters were fixed with 10% neutral buffered formalin (NBF).

Definition of ureter segments in healthy cats

Images of fixed ureters were obtained, and their lengths were measured using ImageJ software (National Institutes of Health, Bethesda, MD, USA). The obtained ureters were divided into four segments and defined as proximal (Pro), middle 1 (Mid1), middle 2 (Mid2), and distal (Dis); the actual distance or the range of segments were more than 6.91 cm, 4.71–6.90 cm, 2.31–4.70 cm, and 0.00–2.30 cm from the ureter-urinary bladder junction, respectively.

Sample preparations from cat clinical cases

Informed consent was obtained from the owners of the animals. The age and BW of the cats were recorded, and blood urea nitrogen (BUN) and serum creatinine (CRE) were measured using a Fuji Dri-Chem biochemistry analyzer (Fujifilm, Tokyo, Japan). The ureters (*n* = 20 cats, 24 ureters) were obtained from cat cases manifesting obstructive urolithiasis in Matsubara Animal Hospital (Matsubara, Japan) that resulted in surgical therapeutic resection. The nature of the urinary calculus was analyzed by the infrared absorption spectroscopy in Osaka Kessei Research Laboratories, Inc. (Osaka, Japan). The resected ureters contained from just proximal portion of obstructed lesions to the ureter-urinary bladder junction, and they were fixed using 10% NBF.

Definition of ureter segments in cat clinical cases

Diseased ureters were divided into four equal parts termed disease parts (dPart) 1–4. The length of each dPart depended on the localization of obstructive lesion and differed among cat cases. Each dPart was mapped to the corresponding segment of the healthy ureter. Briefly, to judge the

correspondence between each dPart and the criteria in healthy ureter segments (Pro, Mid1, Mid2, Dis), the distance from ureter-urinary bladder junction of each dPart was measured and corresponded to the actual distance or the range of segments (6.91 cm, 4.71–6.90 cm, 2.31–4.70 cm, and 0.00–2.30 cm) defined in healthy cats. Further, diseased ureters containing obstructed regions (dUOR) or its distal regions (dUDR) were separately evaluated in histopathological analysis.

Histological analysis

Fixed ureters were dehydrated using alcohol and were embedded in paraffin. Deparaffinized histological cross-sections (2–3-μm-thick) were stained with Masson's trichrome (MT) or immunohistochemistry (IHC). For IHC, sections were incubated in 20 mM Tris-HCl buffer (pH 9.0) for 15 min at 110°C, treated with 0.3% H_2O_2/methanol solution for 20 min, and blocked using 10% normal goat serum (SABPO kit; Nichirei Bioscience, Tokyo, Japan). Sections were incubated overnight with primary antibodies for CD20 (B cell marker; 1:300; E2560, Spring Bioscience, Pleasanton, CA, USA) or IBA1 (macrophage marker; 1:800; 019-19741, FUJIFILM Wako Pure Chemical Corporation, Osaka, Japan) at 4°C. The sections were then treated with biotinylated goat anti-rabbit IgG (SABPO kit; Nichirei Bioscience) for 30 min at room temperature. This was followed by incubation with streptavidin-horseradish peroxidase using the SABPO kit (Nichirei Bioscience) for 30 min, followed by incubation with 3,3-diaminobenzidine tetrahydrochloride. Finally, the sections were counterstained with hematoxylin.

Histoplanimetry

All stained sections were examined using a BZ-X710 microscope (Keyence, Osaka, Japan) and converted to virtual slides using a NanoZoomer 2.0-RS (Hamamatsu Photonics, Shizuoka, Japan). By using MT-stained sections, each component of the ureters, including the adventitia, muscular layer (ML), submucosa (SM), transitional epithelium (TE), and lumen (LU), was analyzed. As the adventitia was compartmentalized into external large and internal narrow layers composed of adipose tissue and collagen fibers, respectively, we focused on the latter, "adventitia composed of collagen fibers (ADCF)." The perimeters of ADCF or ML were measured as thickness indices of the ureters by NDP.view2 (Hamamatsu Photonics). The area of each ureter component was also measured by

NDP.view2, and the percentage of the total ureter area was calculated. For ML development, internal longitudinal ML (Int LL), middle circular ML (Mid CL), external longitudinal ML (Ext LL), and longitudinal ML found in the ADCF (Ad LL) were identified in the sections, and their development was categorized as follows: Glade 0, undeveloped; Glade 1, identifiable but less-developed; Glade 2, clearly identifiable and developed; and Grade 3, clearly identifiable and well-developed. The average grade in the examined sections was expressed as a score for ML development. Further, the number of nerve bundles found in MT-stained sections, and $CD20^+$ or $IBA1^+$ cells in IHC sections were counted in the ureter, and their numbers/examined ureter areas were calculated.

Statistical analysis

All statistical analysis was performed by non-parametric methods using SPSS statistics version 23 (IBM Japan, Ltd., Tokyo, Japan). Mann–Whitney *U*-test was used for two-group comparisons. For multiple comparisons, Dunnett's test or Scheffé's method was performed when statistical significance was observed with the Kruskal–Wallis test. Statistical significance was set at $P < 0.05$.

Results

Body weight and ureter morphology of healthy cats

Table 1 summarizes the information of the examined healthy cats. Body weight, left ureter length, and right ureter length were 4.32 ± 0.18 kg, 8.50 ± 0.35 cm, and 9.88 ± 0.38 cm, respectively. The mean of left and right ureter length was 9.19 ± 0.34 cm.

Histologically, the ureter mucosa was composed of TE and SM, and the lamina muscularis was not present in all segments (Fig. 1A). Well-developed Mid CL and less-developed Int LLs and Ext LLs were observed. ADCF attached to the most external ML, and their development differed among examined ureter segments (Fig. 1A). The outside of the ADCF was covered by adipose tissue in the adventitia. For indices of ureter thickness, the ADCF and CL perimeters were 2.7 and 2.3 mm (Fig. 1B, "Total" showing the mean of all examined segments), and they were similar values among the examined segments. The measured area of each ureter component differed among segments, especially SM in Mid1 or Mid2 was smaller but ADCF in Dis was larger than their corresponding components in Pro (Fig. 1C). Importantly, area of LU was significantly smaller in Mid1 than in Pro when they were analyzed by two-group comparisons (Mann–Whitney *U*-test, $P = 0.02$) although there was no significant difference in multiple comparisons. Figure 1D shows the percentage component of the total ureter area, and SM in Pro had a significantly higher ratio than the other segments. Furthermore, ADCF in Mid2 or Dis had a significantly higher ratio compared to Pro, but there was no segment-related difference in Lu, TE, and CL.

Figure 2 focuses on ML development. The Int LLs and Ext LLs were quite thin and partially observed in all examined ureter regions, whereas longitudinal muscular fibers were also observed in ADCF, termed Ad LL (Fig. 2A). With regard to the morphometry of ML in the entire ureter, the Mid CL was significantly better developed compared to the other layers in both species, and the cat Ad LL was also significantly better developed compared to the Int and Ext LLs (Fig. 2B). For comparison of ML development, the Mid CL in Dis and the Ad LLs in Mid1, Mid2, and Dis were significantly better developed compared to the corresponding MLs in Pro (Fig. 2C). Moreover, the Ad LL in Dis also showed a significantly higher score than Mid1. These data emphasize the morphological differences among cat ureter segments.

196 ***Clinical and ureter information of diseased cats***

197 Table 2 summarizes the information on cats with ureteral urolithiasis. Of the eight males and 12
198 females examined, only one female was intact, and the others were neutered. Almost all cases
199 manifested CaOx urolithiasis, and dried solidified blood stone, magnesium ammonium phosphate,
200 or ammonium acid urate were also detected in one case each. There was no sex-related differences
201 in age (male vs female; 6.56 ± 1.31 vs 7.97 ± 0.93 years, P = 0.427), BW (3.84 ± 0.22 vs 3.63 ± 0.29
202 kg, P = 0.343), BUN (77.96 ± 17.42 vs 97.22 ± 21.39 mg/dL, P = 0.851), CRE (4.36 ± 1.16 vs 7.42 ± 2.01
203 mg/dL, P = 0.571), or dissected ureter length (5.55 ± 0.60 vs 5.74 ± 0.74 cm, P = 1.000).
204
205 ***Histopathological features and size of diseased cat ureters***

206 Diseased ureters were divided into four equal parts (dPart, Fig. 3A), and their histopathological
207 differences were examined. Diseased ureters showed a dilated lumen (Fig. 3B) and increased
208 connective tissues from the SM to the ADCF (Fig. 3C), and these features differed among individual
209 cats or examined parts. For histopathological comparison of each part, dPart1 was the thickest; it
210 decreased toward dPart4, and significance was detected between dPart1 and dPart4 in the ADCF
211 perimeter (Fig. 3D). Further, the area of each component showed a similar tendency with perimeter,
212 and the SM and CL in dPart1 were significantly larger than those in dPart4; there was no part-related
213 differences in LU, TE, and ADCF (Fig. 3E). There were no significant differences in the percentage of
214 total ureter area among the examined parts (Fig. 3F). These data indicate that dPart1, a part close
215 to the obstructed lesion due to urolith, showed a tendency for thickening without the alternation of
216 each composition ratio.
217
218 ***Comparison of ureter size between healthy and diseased cats***

219 Each part of the diseased ureter was mapped to the corresponding segment of the healthy ureter,
220 and dUOR or its distal regions, dUDR, were separately evaluated (Fig. 4A). The mean of all examined
221 segments was calculated, and the diseased ureters were found to be significantly thicker than
222 healthy ureters (Fig. 4B). As for the perimeter of each segment, all examined segments in dUORs
223 tended to show higher values compared to healthy ureters, and significance was detected in the
224 ADCF and CL of Mid1, Mid2, and Dis. The dUDRs showed significantly higher values in the ADCF of

Mid1 and Mid2, and the CL of Mid1. These data indicate the presence of thickened diseased ureters, particularly near obstructed lesions.

Comparison of each component area between healthy and diseased cat ureters

With the exception of LU, the area of all components was significantly larger in diseased ureters than in healthy ureters (Fig. 5A). In terms of the percentage of each ureter component, the ADCF was larger, but the other components were significantly smaller in diseased ureters than in healthy ureters (Fig. 5B). For area comparison in each segment (Fig. 5C), dUORs showed significantly larger ADCF in Pro; ADCF, CL, or SM in Mid1; ADCF or SM in Mid2; and CL or SM in Dis compared to healthy ureters. The dUDRs showed a significantly larger CL in Mid1 than in the healthy ureter. For percentage expression (Fig. 5D), the dUOR showed significantly larger ADCF and smaller SM or LU in Pro; and larger ADCF and smaller SM or TE in Mid1 compared to healthy ureters. Moreover, the dUDRs showed significantly larger ADCF and smaller SM in Mid1, larger ADCF in Mid2, and larger ADCF and smaller SM in Dis compared to healthy ureters.

Comparison of each ML between healthy and diseased cat ureters

The mean of all examined segments was calculated, and diseased ureters showed significantly higher scores for ML development in Int, Ext, and Ad LLs than in healthy ones (Fig. 6A). For each region, dUOR showed significantly better developed Ad LL in Pro; Int or Ext LL in Mid1; and Ext LL in Mid2 compared to healthy ureters (Fig. 6B). Furthermore, dUDR showed better developed Int or Ext LL in Mid2 compared to healthy ureters. Furthermore, dUDR showed better developed Int LL compared to dUOR.

Inflammatory features of diseased cat ureters

In diseased ureters, $CD20^+$ B cells and $IBA1^+$ macrophages infiltrated the ADCF, and the latter were also observed in the SM and TE (Fig. 7A). There was no significant difference in the number of inflammatory cells between each part of the diseased ureter, although dPart1 and dPart2 tended to show high values (Fig. 7B). From the mean of all examined segments, the diseased ureter showed significantly higher $CD20^+$ B cell numbers than the healthy ureter, although $IBA1^+$ macrophages were

abundant in both ureters (Fig. 7C). For each segment, the number of $CD20^+$ B cells tended to be higher in dUORs and dUDRs than in healthy ureters, and significance was detected in Pro and Dis of dUOR (Fig. 7D). No significant increase in urolithiasis was observed in $IBA1^+$ macrophages in Pro, Mid1, and Mid2, but that in Dis of dUORs was significantly higher than that in healthy ureters (Fig. 7E).

Decreased nerve bundles and unique histopathological features of diseased cat ureters

Nerve distributions are crucial for the sensation and movement of the ML. In healthy ureters, nerve bundles were observed in the ADCF, but these were decreased in the ADCF of diseased ureters (Fig. 8A). Moreover, the number of nerve bundles tended to increase from dPart1 to dPart4 (from the obstructed region to its distal regions) in diseased ureters, whereas it was significantly decreased in diseased ureters compared to healthy ureters in mean from all examined segments (Fig. 8B). A similar significant decrease in the diseased ureter was detected in each region, regardless of the obstructed regions (Fig. 8C).

In terms of other pathological characteristics of diseased ureters, the deciduation of TE, its invasion and invagination toward ML, and the formation of mucosal folds were also observed (Fig. 8D).

Discussion

In healthy cat ureters, the Mid CL is the most developed ML among the entire ureter, and its contraction and relaxation mainly contributes to ureteral peristalsis and urine transport (Kiil, 1973). However, in three-dimensional features, ureter MLs run by oblique patterns; therefore, the combined movement of the Mid CL, as well as longitudinal muscular bundles on histological sections might be crucial for urine transportation by ML. Healthy cats show development of ADCF and Ad LL toward ureter-urinary bladder junction, indicating segmental differences in ureter movement. These anatomical and histological features might affect the transport efficiency of urine from the renal pelvis to the urinary bladder. Food and obesity are considered risk factors for urinary organ-associated diseases, including urolithiasis in cats (Gomes et al., 2018; Kocabağlı et al., 2017). In addition, morphological characteristics of ureters, such as differences in relative length and width, or the development of ML and ADCF might affect their pathogenesis.

Diseased cats showed a high incidence rate of urolithiasis due to CaOx calculus. Recently, the incidence of urolithiasis in cats has been increasing due to the aging of animals and the promotion of urine acidifying or animal protein-containing diets (Lulich et al., 2016; Osborne et al., 2009). Furthermore, the present study targeted urolithiasis cases that require surgical dissection of ureters; therefore, cases with CaOx were inevitably included. We found no relationship between urolithiasis development and age, sex, or BW, although these factors are considered to be factors affecting its incidence (Gomes et al., 2018; Kocabağlı et al., 2017). Furthermore, there was no significant correlation between elevated BUN or Cre and age, BW, sex, and dissected ureter length in diseased cats. Therefore, ureteral obstruction of CaOX calculus causes renal dysfunction regardless of age, BW, sex, and the localization of the obstructive region along the ureters.

The diseased cat ureters showed dilated or fibrotic features, which differed among the cases. In common findings, diseased ureters significantly increased perimeters due to the enlarged area of each component, developed LLs, abundant inflammatory cells, and decreased nerve bundles in ADCF. In particular, an increase in the ADCF perimeter and area of the SM and CL were observed in dPart1, a part close to the obstructed lesion. MT staining also revealed increased collagen fibers in SM, intermuscular spaces, and ADCF in diseased ureters, and these connective tissue developments also affect their area increase in dPart1. During the progression of fibrosis, inflammation also affects its

pathogenesis in various organs (Distler et al., 2019); however, we found no significant difference in inflammation scores among dParts1–4, although a decreasing tendency from dPart1 to dPart4 was observed. Therefore, in addition to inflammation, other factors, such as physical stimulation or pressure by CaOx calculus, cause severe alterations in ureter morphology in dPart1.

The mean value of the dissected ureter length is 5.66 ± 0.49 cm, and our results suggest that Mid1 (4.71–6.90 cm) has the highest risk of CaOx calculus obstruction. In the healthy cat ureter, the perimeter and total area were smallest in Mid1 among the examined segments; in particular, the SM area was significantly smaller in Mid1 than in Pro. The ureter SM has developed collagen fibers and contributes to the adaptation to mucosal morphological changes associated with ureteral movement (Kiil, 1973; Takaddus et al., 2016). Furthermore, LU area was significantly decreased from Pro to Mid1 in two group comparisons in healthy cat ureters. Therefore, the size decrease of the ureter, LU, and SM from Pro to Mid1 might create an environment that is prone to blockages of CaOx calculus.

As for the difference in histopathological features in each ureter segment, Mid1 showed remarkable morphological changes, such as ureter size indices and each component area in both dUOR and dUDR. These data suggest that Mid is sensitive to alterations in its structures in both Pro and Mid1 obstructions. Further, the area from ADCF to SM tended to increase, regardless of the segments or obstruction localizations. Characteristically, Ad LL was clearly observed in healthy cats from Mid1 onward, and longitudinal muscular layers tended to develop more frequently in diseased cats compared to healthy cats. Therefore, rather than the development of individual longitudinal muscle itself, the longitudinal muscle layer appears to develop as the developed connective tissue separates the oblique muscle bundles during urolithiasis. In particular, the ADCF increase seemed to principally contribute to this process. Furthermore, nerve bundles observed in ADCF were significantly decreased in diseased cats, regardless of the localization of the segment or obstruction. Ureters innervate the sympathetic nerves from the thoracic or lumbar spinal cords, parasympathetic nerves from the vagus nerve or pelvic nerve, and sensory nerves (Elbadawi and Schenk, 1969; Feher et al., 1981). Therefore, the nerve decrease is associated with the ADCF alternations with urolithiasis, and may also be associated with nerve dysfunction.

We also revealed TE-related alterations in urolithiasis. In general, CaOx stones show rough surface (Khan et al., 2016); therefore, it might physically damage the ureteral TE. In fact, the human

patients with upper urinary tract urolithiasis had significantly lower expression of tight junction proteins including E-cadherin and tight junction protein 1 with morphological alternations (Jiang and Kuo, 2014). Importantly, lack of TE was observed in several diseased cat ureters, indicating urine leakage to the ureter parenchyma. Urine-leakage has not been evaluated in urolithiasis ureters but is usually observed in trauma of the kidney, ureters, urinary bladder, and urethra (Moores et al., 2002; Titton et al., 2003), and in the obstructed renal pelvis (Mitchinson and Bird, 1971). Furthermore, TE-invasion to the adventitia, and the formation of longitudinal mucosal folds were observed in cat cases. The proliferative features of TE are observed in polypoid/papillary cystitis caused by a reactive proliferative lesion, and they are associated with irritation or injury from calculi, urinary outflow obstruction, ischemia, and inflammatory conditions (Samaratunga et al., 2021). Papillary urothelial hyperplasia/urothelial proliferation is also known to occur in the urinary bladder (Samaratunga et al., 2021). Although there are few reports about similar pathological changes in ureters, the histopathological features found in cat urolithiasis might be related to these TE alterations. In cases showing TE invasion to the adventitia, surgical procedures involving elimination of adipose tissues during resection of the ureter should consider the preservation of ADCF to avoid ureter perforation.

Taken together, our study clarified the morphological characteristics of cat ureters, and their histopathological features in CaOx-urolithiasis. In particular, the size decrease of the ureter, LU, and SM from Pro to Mid1 in healthy ureters and ADCF alternation in diseased ureters, including increased connective tissues with inflammation and decreased nerve bundles, were suggested to be a crucial to consider the pathogenesis of feline ureteral obstruction.

Tables

Table 1. Body weights and ureter lengths in healthy cats.

Parameters	Value
Body weight	4.32 ± 0.18 kg
Left ureter length	8.50 ± 0.35 cm
Right ureter length	9.88 ± 0.38 cm
Mean of left and right ureter lengths	9.19 ± 0.34 cm

Value = mean ±standard error. n = 4, male, mixed breed.

356 **Table 2. General and clinical information and ureter length in the cats showing urolithiasis.**

ID	Breed	Sex	Urolith type	Left or Right ureter	Age	Body weight	BUN	CRE	Dissected ureter length[#]
1	Somali	Cast	Calcium oxalate	Unknown	10.75	2.58	57.90	3.10	7.21
2	Mix	Cast	Calcium oxalate	Unknown	5.42	3.65	68.70	3.10	6.71
3	Mix	Cast	Calcium oxalate	Unknown	9.58	3.60	36.90	2.10	4.75
4	Ragdoll	Cast	Calcium oxalate	Left	4.92	3.60	136.80	6.30	6.87
5	Mix	Cast	Dried solidified blood stone, Calcium oxalate	Unknown	11.83	4.60	45.60	1.71	6.10
6	Scottish Fold	Cast	Calcium oxalate	Unknown	5.33	4.08	32.30	2.01	5.25
7	Munchkin	Cast	Calcium oxalate	Unknown	2.83	4.32	168.60	11.44	1.89
8	Mix*	Cast	Calcium oxalate	Left	1.83	4.30	76.90	5.15	5.58
9	Mix*	Cast	Calcium oxalate	Right	1.83	4.30	76.90	5.15	3.84
			Male	**Mean**	**6.56**	**3.84**	**77.96**	**4.36**	**5.55**
				SE	**1.31**	**0.22**	**17.42**	**1.16**	**0.60**
10	Mix	Spay	Calcium oxalate	Right	2.75	2.78	35.00	1.45	6.60
11	Norwegian Forest	Spay	Magnesium ammonium phosphate	Unknown	10.58	5.80	41.30	2.60	11.00
12	Scottish Fold	Spay	Calcium oxalate	Right	11.75	2.00	140.00	13.80	4.67
13	Mix*	Spay	Calcium oxalate	Right	10.00	4.20	262.80	22.20	3.73
14	Mix*	Spay	Calcium oxalate	Left	10.00	4.20	262.80	22.20	3.73
15	Ragdoll	Spay	Calcium oxalate	Unknown	5.17	3.82	182.70	16.60	5.07
16	Scottish Fold*	Spay	Calcium oxalate	Left	7.75	3.50	140.00	11.50	8.27
17	Scottish Fold*	Spay	Calcium oxalate	Right	7.75	3.50	140.00	11.50	1.64
18	American Shorthair	Female	Calcium oxalate	Unknown	4.50	3.10	37.10	1.70	7.44
19	Mix	Spay	Calcium oxalate	Unknown	13.42	3.55	92.80	7.20	6.07
20	Russian Blue*	Spay	Calcium oxalate	Left	5.75	3.45	54.20	2.30	2.18
21	Russian Blue*	Spay	Calcium oxalate	Right	5.75	3.45	54.20	2.30	2.55
22	Mix	Spay	Calcium oxalate, Ammonium acid urate	Unknown	6.17	4.85	24.30	2.10	2.48
23	Mix	Spay	Calcium oxalate	Unknown	7.83	2.65	119.80	4.52	3.98
24	Mix	Spay	Calcium oxalate	Unknown	10.00	3.90	36.60	3.06	7.35
			Female	**Mean**	**7.97**	**3.63**	**97.22**	**7.42**	**5.74**
				SE	**0.93**	**0.29**	**21.39**	**2.01**	**0.74**
			Male and Female	**Mean**	**7.41**	**3.72**	**89.52**	**6.20**	**5.66**
				SE	**0.76**	**0.19**	**14.43**	**1.31**	**0.49**

*: These ureters are analyzed in same cats. BUN: blood urea nitrogen. CRE: serum creatinine. SE: standard error. #: Ureters are dissected from obstructed lesion to junction with the urinary bladder.

Figure legends

Figure 1. Histological features of the ureters in healthy cats

A: Histology of the ureters. The ureters were examined in each segment, and defined as proximal (Pro), middle 1 (Mid1), middle 2 (Mid2), and distal (Dis). Masson's trichrome staining.

B: Indices of ureter perimeters examined in adventitia composed of collagen fibers (ADCF) or circular muscular layer (CL).

C: Area of each ureter component.

D: Area ratio of each ureter component expressed by percentage.

"Total" indicates the mean of all segments. Values = mean ± standard error. *n* = 8 ureters. Scheffe's method among Pro, Mid1, Mid2, and Dis following significance in the Kruskal-Wallis test. P, P*: significance with Pro ($P < 0.05$, $P < 0.01$). LU: lumen. TE: transitional epithelium. SM: submucosa.

Figure 2. Histological features of the ureter muscular layer s in healthy cats

A: Histology of ureters. The insets show magnification of the square areas of internal longitudinal muscular layer (ML) (Int LL)[1] and external longitudinal ML (Ext LL)[2]. Arrowheads: longitudinal muscular fibers. Arrows: longitudinal muscular fibers in adventitia composed of collagen fibers (Ad LL). Mid CL: middle circular ML. Dotted lines in insets: borders between Mid CL and Int LL or Ext LL. Masson's trichrome staining.

B: Semi-quantitative indices of ureter ML development. "Total" indicates the mean of all segments.

C: Semi-quantitative indices of ML development in each ureter component.

Values = mean ± standard error. *n* = 8 ureters. Scheffe's method following significance in the Kruskal-Wallis test. IL, ML, EL, AL: significance with Int LL, Mid CL, Ext LL, and Ad LL ($P < 0.05$) (B). P: proximal. M1: middle 1. M2: middle 2. D: distal P, M1: significance with P, M1 ($P < 0.05$) (C). Asterisks in addition to the letters indicate high significance ($P < 0.01$) (B and C).

Figure 3. Histopathological features of cat ureters showing urolithiasis

A: Resected ureters in cats with urolithiasis. Ureters were examined by dividing them into four equal parts termed "disease parts (dParts) 1–4". Gross anatomical features.

B and C: Histopathology of ureters in cats with urolithiasis. Dilated (B) and fibrotic (C) cases. Masson's trichrome staining.

D: Indices of ureter perimeters examined in adventitia composed of collagen fibers (ADCF) or circular muscular layer (CL).

E: Area of each ureter component.

F: Area ratio of each ureter component expressed by percentage.

Values = mean ± standard error. *n* = 24 ureters. Dunnett's test with dPart1 following significance in the Kruskal-Wallis test. P4: significance with dPart4 ($P < 0.05$) (D and E). LU: lumen. TE: transitional epithelium. SM: submucosa.

Figure 4. Perimeters of cat ureters showing urolithiasis

A: Illustration for diseased ureter analysis. Diseased ureters were analyzed by defining each obtained part to proximal (Pro), middle 1 (Mid1), middle 2 (Mid2), and distal (Dis), according to the distance from the ureter-urinary bladder junction using the segment definition of healthy cat samples. Diseased ureters containing an obstructed region (dUOR) and diseased ureters distal from the obstructed region (dUDR) were examined separately. "Type" indicates an example for each type of examined samples.

B: Indices of ureter perimeters examined in the adventitia composed of collagen fibers (ADCF) or circular muscular layer (CL). "Total" indicates the mean of all segments. Values = mean ± standard error. *n* = 8 (healthy ureters) and 24 (diseased ureters). Mann-Whitney *U*-test. **: Significance with healthy ureter ($P < 0.01$).

C: Indices of ureter perimeters examined in each segment. Values = mean ± standard error. *n* (ureter number for healthy, dUOR, dUDR) = 8, 5, 0 (Pro); 8, 9, 10 (Mid1); 8, 6, 24 (Mid2); 8, 3, 35 (Dis). Mann–Whitney *U*-test (Pro). Scheffé's method following significance in the Kruskal–Wallis test (Mid1, Mid2, Dis) among healthy, dUOR, and dUDR. *, **: Significance with healthy ureter ($P < 0.05$, $P < 0.01$).

Figure 5. Area of each ureter component in the cat showing urolithiasis.

A: Area of each ureter component.

B: Area ratio of each ureter component expressed by percentage.

414 “Total” indicates the mean of all segments. Values = mean ± SE. *n* = 8 (healthy ureters) and *n* = 24
415 (diseased ureters). Mann–Whitney *U*-test. *, **: Significance with healthy ureter (*P* < 0.05, 0.01).
416 **C**: Area of each ureter component in each segment.
417 **D**: Area ratio of each ureter component expressed by percentage in each segment.
418 Each obtained part was defined as proximal (Pro), middle 1 (Mid1), middle 2 (Mid2), and distal (Dis),
419 according to the distance from the ureter-urinary bladder junction using to the segment definition
420 of healthy cat samples. Diseased ureters containing an obstructed region (dUOR) and diseased
421 ureters distal from the obstructed region (dUDR) were examined separately.
422 Values = mean ± standard error. *n* (ureter number for healthy (HC), dUOR, dUDR) = 8, 5, 0 (Pro); 8, 9,
423 10 (Mid1); 8, 6, 24 (Mid2); 8, 3, 35 (Dis). Mann–Whitney *U*-test (Pro). Scheffé's method following
424 significance in the Kruskal-Wallis test (Mid1, Mid2, Dis) among HC, dUOR, and dUDR. *, **:
425 Significance with HC (*P* < 0.05, *P* < 0.01). LU: lumen. TE: transitional epithelium. SM: submucosa. CL:
426 circular muscular layer. ADCF: adventitia composed of collagen fibers.
427
428 **Figure 6. Muscular layer of the ureter in cats showing urolithiasis**
429 **A**: Semi-quantitative indices of ureter muscular layer (ML) development. “Total” indicates the mean
430 of all segments. Values = mean ± standard error. *n* = 8 (healthy ureters) and 24 (diseased ureters).
431 Mann–Whitney *U*-test. *, **: Significance with healthy ureter (*P* < 0.05, 0.01).
432 **B**: Semi-quantitative indices of ureter ML development in each segment.
433 Each obtained part was defined as proximal (Pro), middle 1 (Mid1), middle 2 (Mid2), and distal (Dis),
434 according to the distance from the ureter-urinary bladder junction using the segment definition of
435 healthy cat samples. Diseased ureters containing an obstructed region (dUOR) and diseased ureters
436 distal from the obstructed region (dUDR) were examined separately.
437 Values = mean ± standard error. *n* (ureter number for healthy, dUOR, dUDR) = 8, 5, 0 (Pro); 8, 9, 10
438 (Mid1); 8, 6, 24 (Mid2); 8, 3, 35 (Dis). Mann–Whitney *U*-test (Pro). Scheffé's method following
439 significance in the Kruskal–Wallis test (Mid1, Mid2, Dis). *, **: Significance with healthy ureter (*P* <
440 0.05, *P* < 0.01). ##: Significance with dUDR (*P* < 0.01).
441
442 **Figure 7. Inflammation of the ureter in the cat showing urolithiasis**

A: Localization of $CD20^+$ B cells and $IBA1^+$ macrophages in the diseased ureters. Immunohistochemistry. LU: lumen. TE: transitional epithelium. SM: submucosa. CL: circular muscular layer. ADCF: adventitia composed of collagen fibers.

B: Number of $CD20^+$ B cells and $IBA1^+$ macrophages in each ureter. Ureters were examined by dividing them into four equal parts termed "disease parts (dParts) 1–4". Values = mean ± standard error. *n* = 24 ureters.

C: Number of $CD20^+$ B cells and $IBA1^+$ macrophages in each ureter. Ureters were examined by dividing them into four equal parts termed "dParts 1–4". "Total" indicates the mean of all segments. Values = mean ± standard error. *n* = 8 (healthy ureters) and 24 (diseased ureters). Mann–Whitney *U*-test. *, **Significance with healthy ureter ($P < 0.01$).

D: Number of $CD20^+$ B cells in each ureter segment.

E: Number of $IBA1^+$ macrophages in each ureter segment.

Each obtained part was defined as proximal (Pro), middle 1 (Mid1), middle 2 (Mid2), and distal (Dis), according to the distance from the ureter-urinary bladder junction using the segment definition of healthy cat samples. Diseased ureters containing an obstructed region (dUOR) and diseased ureters distal from the obstructed region (dUDR) were examined separately.

Values = mean ± standard error. *n* (ureter number for healthy (HC), dUOR, dUDR) = 8, 5, 0 (Pro); 8, 9, 10 (Mid1); 8, 6, 24 (Mid2); 8, 3, 35 (Dis). Mann–Whitney *U*-test (Pro). Scheffé's method following significance in the Kruskal–Wallis test (Mid1, Mid2, Dis) among HC, dUOR, and dUDR. *, **: Significance with HC ($P < 0.05$, $P < 0.01$).

Figure 8. Histopathological characteristics found in the ureter of cats showing urolithiasis.

A: Nerve bundles found in the ureter adventitia in healthy and diseased cats. Arrows: nerve bundles. Masson's trichrome staining.

B: Number of nerve bundles in each ureter. The ureters were examined by dividing them into four equal parts termed "disease parts (dParts) 1–4", left panel. The right panel indicates the mean of all the parts. Values = mean ± standard error (*n* = 24 ureters). Mann–Whitney *U*-test. **: Significance with healthy ureter ($P < 0.01$).

C: Number of nerve bundles in each ureter segment.

Each obtained part was defined as proximal (Pro), middle 1 (Mid1), middle 2 (Mid2), and distal (Dis), according to the distance from the ureter-urinary bladder junction using the segment definition of healthy cat samples. Diseased ureters containing an obstructed region (dUOR) and diseased ureters distal from the obstructed region (dUDR) were examined separately.

Values = mean ± standard error. *n* (ureter number for healthy (HC), dUOR, dUDR) = 8, 5, 0 (Pro); 8, 9, 10 (Mid1); 8, 6, 24 (Mid2); 8, 3, 35 (Dis). **Significance with HC ($P < 0.01$). Scheffé's method following significance in the Kruskal–Wallis test (Mid1, Mid2, Dis).

D: Characteristic features found in ureters of cats with urolithiasis. Transitional epithelium (TE) deciduation (upper panels), TE invasion (lower left panel), and mucosal fold formation (lower right panel) were observed. Masson’s trichrome staining.

Author Contributions

OI, KO, and YK conceptualized the study design. OI designed the experiments. OI, KO, HM, NY, TaN, YO, and NS performed the sampling and experiments. OI and TeN analyzed the data. All authors reviewed and discussed the results and contributed to the preparation of the manuscript. YK supervised the project.

Acknowledgements

None.

Data Availability

The data that support the findings of this study are available from the corresponding author upon reasonable request.

Disclosures

The authors declare no competing interests.

Funding

This work was supported by JSPS KAKENHI Grant Numbers 19K22352 and 21H04751.

References

1. Berent, A.C., Weisse, C.W., Bagley, D.H., Lamb, K., 2018. Use of a subcutaneous ureteral bypass device for treatment of benign ureteral obstruction in cats: 174 ureters in 134 cats (2009–2015). *J. Am. Vet. Med. Assoc*. **253**, 1309–1327.
2. Brourman, J.D., 2011. Successful replacement of an obstructed ureter with an ileal graft in a cat. *J. Am. Vet. Med. Assoc*. **238**, 1173–1175.
3. Distler, J.H.W., Györfi, A.H., Ramanujam, M., Whitfield, M.L., Königshoff, M., Lafyatis, R., 2019. Shared and distinct mechanisms of fibrosis. *Nat. Rev. Rheumatol.* **15**, 705-730.
4. Dorsch, R., Remer, C., Sauter-Louis, C., Hartmann, K., 2014. Feline lower urinary tract disease in a German cat population. A retrospective analysis of demographic data, causes and clinical signs. *Tierarztl. Prax. Ausg. K. Kleintiere. Heimtiere.* **42**, 231–239.
5. Dru Forrester, S., Roudebush, P., 2007. Evidence-Based Management of Feline Lower Urinary Tract Disease. *Vet. Clin. North Am. - Small Anim. Pract.* **37**, 533–558.
6. Elbadawi, A., Schenk, E.A., 1969. Innervation of the abdominopelvic ureter in the cat. *Am. J. Anat*. **126**, 103–119.
7. Feher, E., Salimova, N.B., Sakharov, D.A., Vajda, J., 1981. Innervation of the cat ureter. An experimental study. *Acta Morphol. Acad. Sci. Hung.* **29**, 353–359.
8. Finch, N.C., 2016. Hypercalcaemia in cats: The complexities of calcium regulation and associated clinical challenges. *J. Feline Med. Surg.* **18**, 387–399.
9. Gomes, V.R., Ariza, P.C., Borges, N.C., Schulz, F.J., Fioravanti, M.C.S., 2018. Risk factors associated with feline urolithiasis. *Vet. Res. Commun.* **42**, 87–94.
10. Houston, D.M., Moore, A.E.P., 2009. Canine and feline urolithiasis: Examination of over 50000 urolith submissions to the Canadian Veterinary Urolith centre from 1998 to 2008. *Can. Vet. J.* **50**, 1263–1268.
11. Jiang, Y.H., Kuo, H.C., 2014. Urothelial Dysfunction and Increased Suburothelial Inflammation of Urinary Bladder Are Involved in Patients with Upper Urinary Tract Urolithiasis – Clinical and Immunohistochemistry Study. *PLoS One* **9**, e110754.
12. Kaul, E., Hartmann, K., Reese, S., Dorsch, R., 2020. Recurrence rate and long-term course of cats with feline lower urinary tract disease. *J. Feline Med. Surg*. **22**, 544–556.
13. Khan, S.R., Pearle, M.S., Robertson, W.G., Gambaro, G., Canales, B.K., Doizi, S., Traxer, O., Tiselius, H.G., 2016. Kidney stones. *Nat. Rev. Dis. Prim.* **2**, 16008.
14. Kiil, F., 1973. Urinary Flow and Ureteral Peristalsis, in: Wolfgang, L., Hannappel, J. (Eds.), Urodynamics. *Springer,* Berlin, Germany, pp. 57–70.

15. Kocabağlı, N., Kutay, H.C., Dokuzeylül, B., Süer, İ.N.E., Apt, M., 2017. The Analysis of Computer Data regarding Obesity and Associated Diseases in Cats Examined at Private Veterinary Practices. *Acta Sci. Vet*. **45**, 1506.
16. Lewis, T.W., Wiles, B.M., Llewellyn-Zaidi, A.M., Evans, K.M., O'Neill, D.G., 2018. Longevity and mortality in Kennel Club registered dog breeds in the UK in 2014. *Canine Genet. Epidemiol.* **5**, 1–17.
17. Lulich, J.P., Berent, A.C., Adams, L.G., Westropp, J.L., Bartges, J.W., Osborne, C.A., 2016. ACVIM Small Animal Consensus Recommendations on the Treatment and Prevention of Uroliths in Dogs and Cats. *J. Vet. Intern. Med.* **30**, 1564–1574.
18. Mitchinson, M.J., Bird, D.R., 1971. Urinary leakage and retroperitoneal fibrosis. *J. Urol.* **105**, 56–58.
19. Moores, A.P., Bell, A.M.D., Costello, M., 2002. Urinoma (para-ureteral pseudocyst) as a consequence of trauma in a cat. *J. Small Anim. Pract.* **43**, 213–216.
20. Nesser, V.E., Reetz, J.A., Clarke, D.L., Aronson, L.R., 2018. Radiographic distribution of ureteral stones in 78 cats. *Vet. Surg.* **47**, 895–901
21. O'Neill, D.G., Church, D.B., McGreevy, P.D., Thomson, P.C., Brodbelt, D.C., 2015. Longevity and mortality of cats attending primary care veterinary practices in England. *J. Feline Med. Surg.* **17**, 125–133.
22. Osborne, C.A., Klausner, J.S., Lees, G.E., 1979. Urinary tract infections: Normal and abnormal defense mechanisms. *Vet. Clin. North Am. - Small Anim. Pract*. **9**, 587–609.
23. Osborne, C.A., Lulich, J.P., Forrester, D., Albasan, H., 2009. Paradigm Changes in the Role of Nutrition for the Management of Canine and Feline Urolithiasis. *Vet. Clin. North Am. - Small Anim. Pract*. **39**, 127–141.
24. Samaratunga, H., Delahunt, B., Yaxley, J., Egevad, L., 2021. Tumour-like lesions of the urinary bladder. *Pathology.* **53**, 44–55.
25. Takaddus, A.T., Gautam, P., Chandy, A.J., 2016. Numerical simulations of peristalsis in unobstructed human ureters, in: ASME International Mechanical Engineering Congress and Exposition, Proceedings (IMECE). *American Society of Mechanical Engineers (ASME).* **3**, V003T04A024.
26. Titton, R.L., Gervais, D.A., Hahn, P.F., Harisinghani, M.G., Arellano, R.S., Mueller, P.R., 2003. Urine Leaks and Urinomas: Diagnosis and Imaging-guided Intervention. *Radiographics*. **23**, 1133–1147.

Table 1

Parameters	Value
Body weight	4.32 ± 0.18 kg
Left ureter length	8.50 ± 0.35 cm
Right ureter length	9.88 ± 0.38 cm
Mean of left and right ureter length	9.19 ± 0.34 cm

Value = mean ± standard error. n = 4, male, mixed breed.

Figure 1

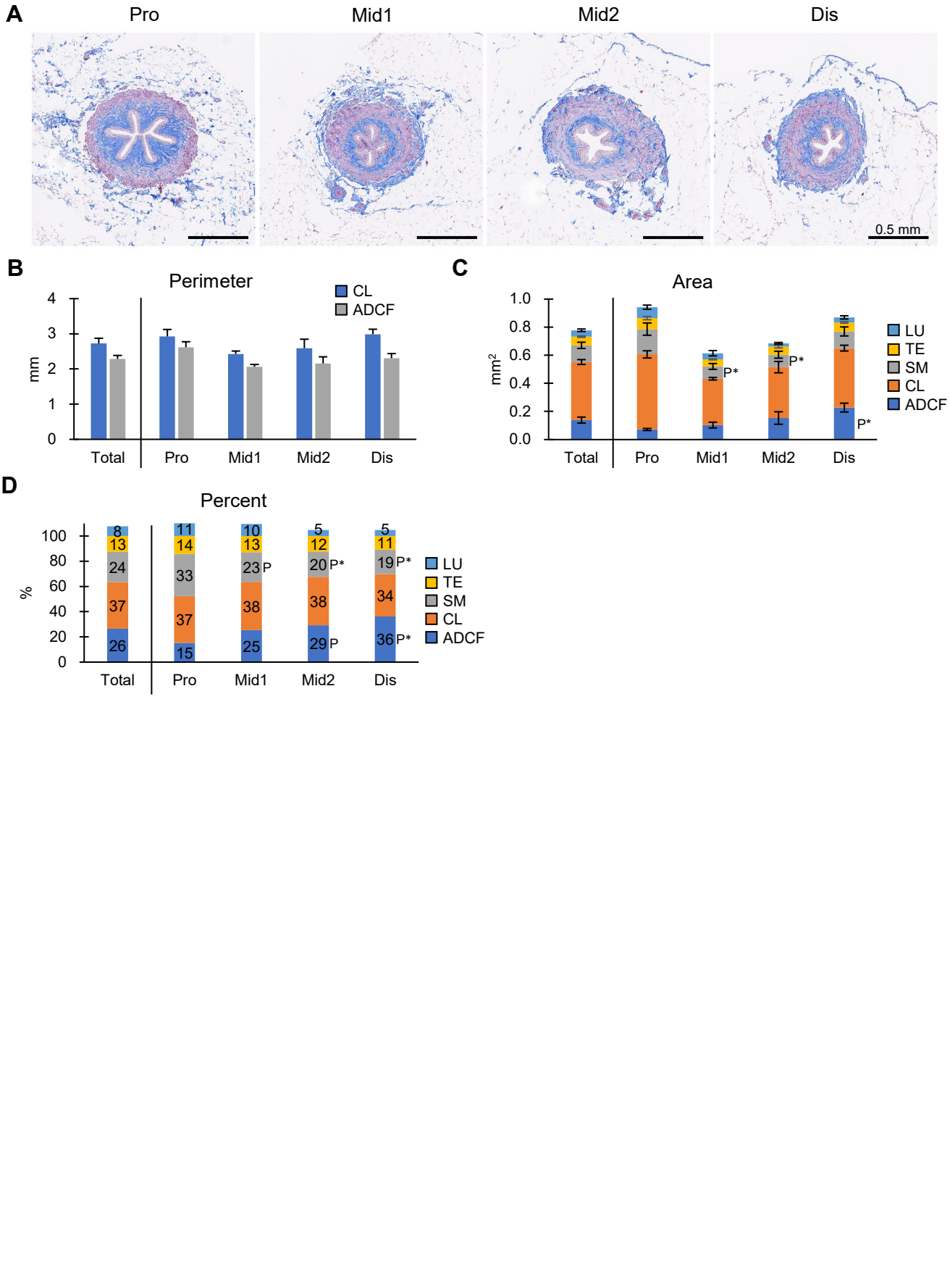
A
Pro
Mid1
Mid2
Dis
0.5 mm
B
Perimeter
CL
ADCF
mm
4
3
2
1
0
Total
Pro
Mid1
Mid2
Dis
C
Area
mm²
1.0
0.8
0.6
0.4
0.2
0.0
P*
LU
TE
SM
CL
ADCF
D
Percent
%
100
80
60
40
20
0
8
13
24
37
26
11
14
33
37
15
10
13
23 P
38
25
5
12
20 P*
38
29 P
5
11
19 P*
34
36 P*

Figure 2

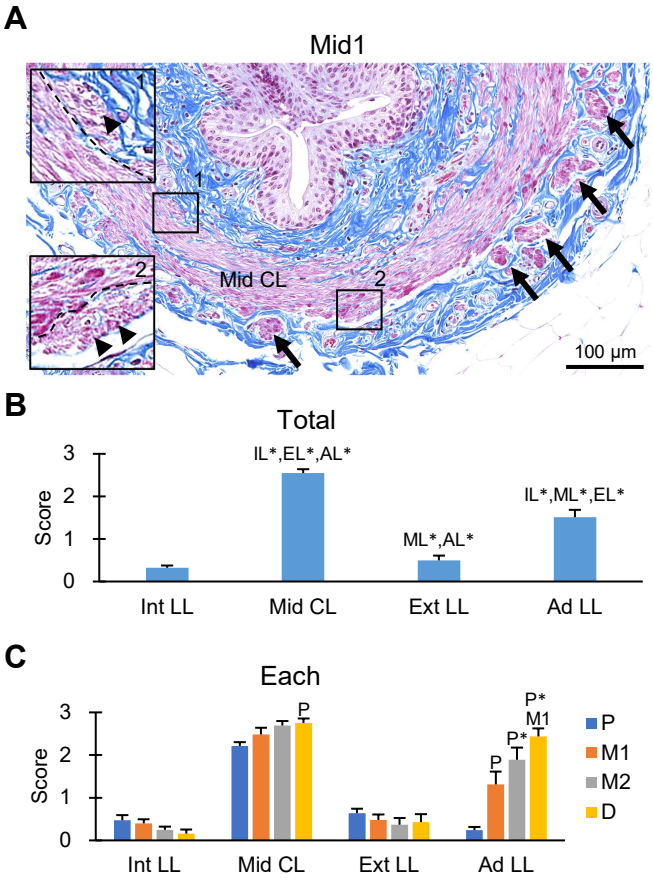
A
Mid1
1
1
2
2
Mid CL
100 μm
B
Total
Score
3
2
1
0
IL*,EL*,AL*
ML*,AL*
IL*,ML*,EL*
Int LL
Mid CL
Ext LL
Ad LL
C
Each
Score
3
2
1
0
P
P
P*
P*
M1
Int LL
Mid CL
Ext LL
Ad LL
P
M1
M2
D

Table 2

ID	Breed	Sex	Urolith type	Left or Right ureter	Age	Body weight	BUN	Cre	Dissected ureter length[#]
1	Somali	Cast	Calcium oxalate	Unknown	10.75	2.58	57.90	3.10	7.21
2	Mix	Cast	Calcium oxalate	Unknown	5.42	3.65	68.70	3.10	6.71
3	Mix	Cast	Calcium oxalate	Unknown	9.58	3.60	36.90	2.10	4.75
4	Ragdoll	Cast	Calcium oxalate	Left	4.92	3.60	136.80	6.30	6.87
5	Mix	Cast	Dried solidified blood stone, Calcium oxalate	Unknown	11.83	4.60	45.60	1.71	6.10
6	Scottish Fold	Cast	Calcium oxalate	Unknown	5.33	4.08	32.30	2.01	5.25
7	Munchkin	Cast	Calcium oxalate	Unknown	2.83	4.32	168.60	11.44	1.89
8	Mix*	Cast	Calcium oxalate	Left	1.83	4.30	76.90	5.15	5.58
9	Mix*	Cast	Calcium oxalate	Right	1.83	4.30	76.90	5.15	3.84
			Male	**Mean**	**6.56**	**3.84**	**77.96**	**4.36**	**5.55**
				SE	**1.31**	**0.22**	**17.42**	**1.16**	**0.60**
10	Mix	Spay	Calcium oxalate	Right	2.75	2.78	35.00	1.45	6.60
11	Norwegian Forest	Spay	Magnesium ammonium phosphate	Unknown	10.58	5.80	41.30	2.60	11.00
12	Scottish Fold	Spay	Calcium oxalate	Right	11.75	2.00	140.00	13.80	4.67
13	Mix*	Spay	Calcium oxalate	Right	10.00	4.20	262.80	22.20	3.73
14	Mix*	Spay	Calcium oxalate	Left	10.00	4.20	262.80	22.20	3.73
15	Ragdoll	Spay	Calcium oxalate	Unknown	5.17	3.82	182.70	16.60	5.07
16	Scottish Fold*	Spay	Calcium oxalate	Left	7.75	3.50	140.00	11.50	8.27
17	Scottish Fold*	Spay	Calcium oxalate	Right	7.75	3.50	140.00	11.50	1.64
18	American Shorthair	Female	Calcium oxalate	Unknown	4.50	3.10	37.10	1.70	7.44
19	Mix	Spay	Calcium oxalate	Unknown	13.42	3.55	92.80	7.20	6.07
20	Russian Blue*	Spay	Calcium oxalate	Left	5.75	3.45	54.20	2.30	2.18
21	Russian Blue*	Spay	Calcium oxalate	Right	5.75	3.45	54.20	2.30	2.55
22	Mix	Spay	Calcium oxalate, Ammonium acid urate	Unknown	6.17	4.85	24.30	2.10	2.48
23	Mix	Spay	Calcium oxalate	Unknown	7.83	2.65	119.80	4.52	3.98
24	Mix	Spay	Calcium oxalate	Unknown	10.00	3.90	36.60	3.06	7.35
			Female	**Mean**	**7.97**	**3.63**	**97.22**	**7.42**	**5.74**
				SE	**0.93**	**0.29**	**21.39**	**2.01**	**0.74**
			Male and Female	**Mean**	**7.41**	**3.72**	**89.52**	**6.20**	**5.66**
				SE	**0.76**	**0.19**	**14.43**	**1.31**	**0.49**

*: These ureters are analyzed in same cats. BUN: blood urea nitrogen. Cre: serum creatinine. SE: standard error. #: Ureters are dissected from obstructed lesion to junction with the urinary bladder.

Figure 3

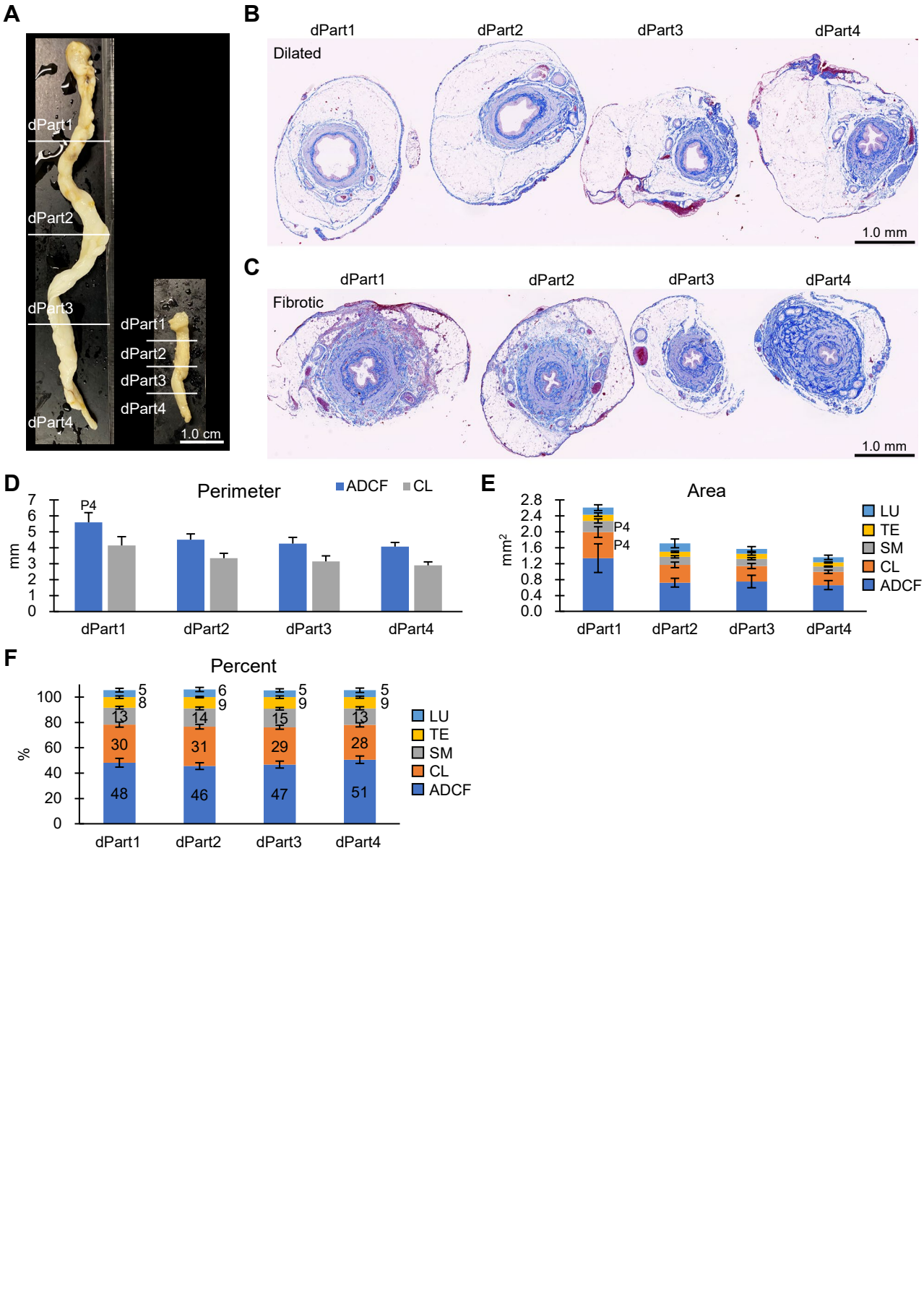
A
dPart1
dPart2
dPart3
dPart4
1.0 cm
B
dPart1
dPart2
dPart3
dPart4
Dilated
1.0 mm
C
dPart1
dPart2
dPart3
dPart4
Fibrotic
1.0 mm
D
Perimeter
ADCF
CL
mm
P4
dPart1
dPart2
dPart3
dPart4
E
Area
mm2
P4
P4
LU
TE
SM
CL
ADCF
dPart1
dPart2
dPart3
dPart4
F
Percent
%
48
30
13
8
5
46
31
14
9
6
47
29
15
9
5
51
28
13
9
5
LU
TE
SM
CL
ADCF
dPart1
dPart2
dPart3
dPart4

Figure 4

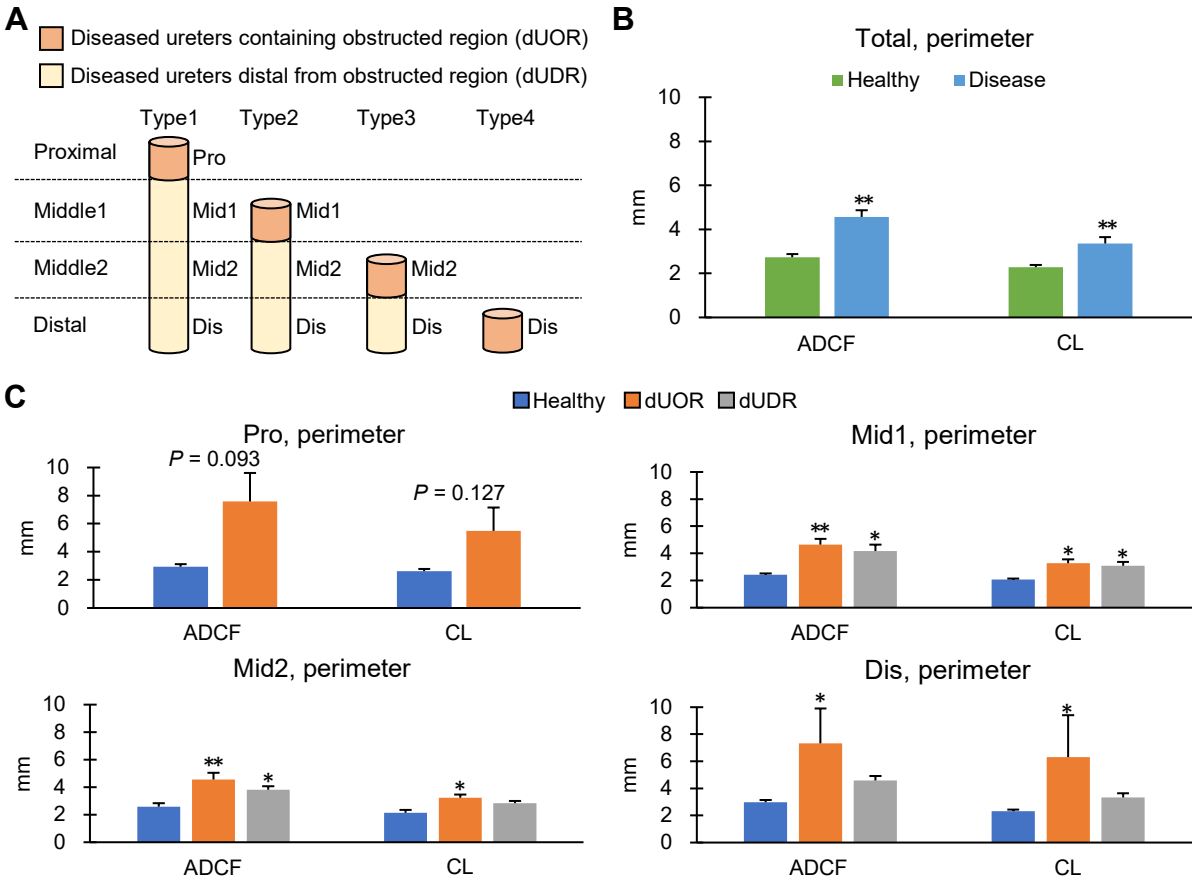
A
Diseased ureters containing obstructed region (dUOR)
Diseased ureters distal from obstructed region (dUDR)
Type1
Type2
Type3
Type4
Proximal
Middle1
Middle2
Distal
Pro
Mid1
Mid2
Dis
B
Total, perimeter
Healthy
Disease
mm
ADCF
CL
C
Healthy
dUOR
dUDR
Pro, perimeter
P = 0.093
P = 0.127
Mid1, perimeter
Mid2, perimeter
Dis, perimeter

Figure 5

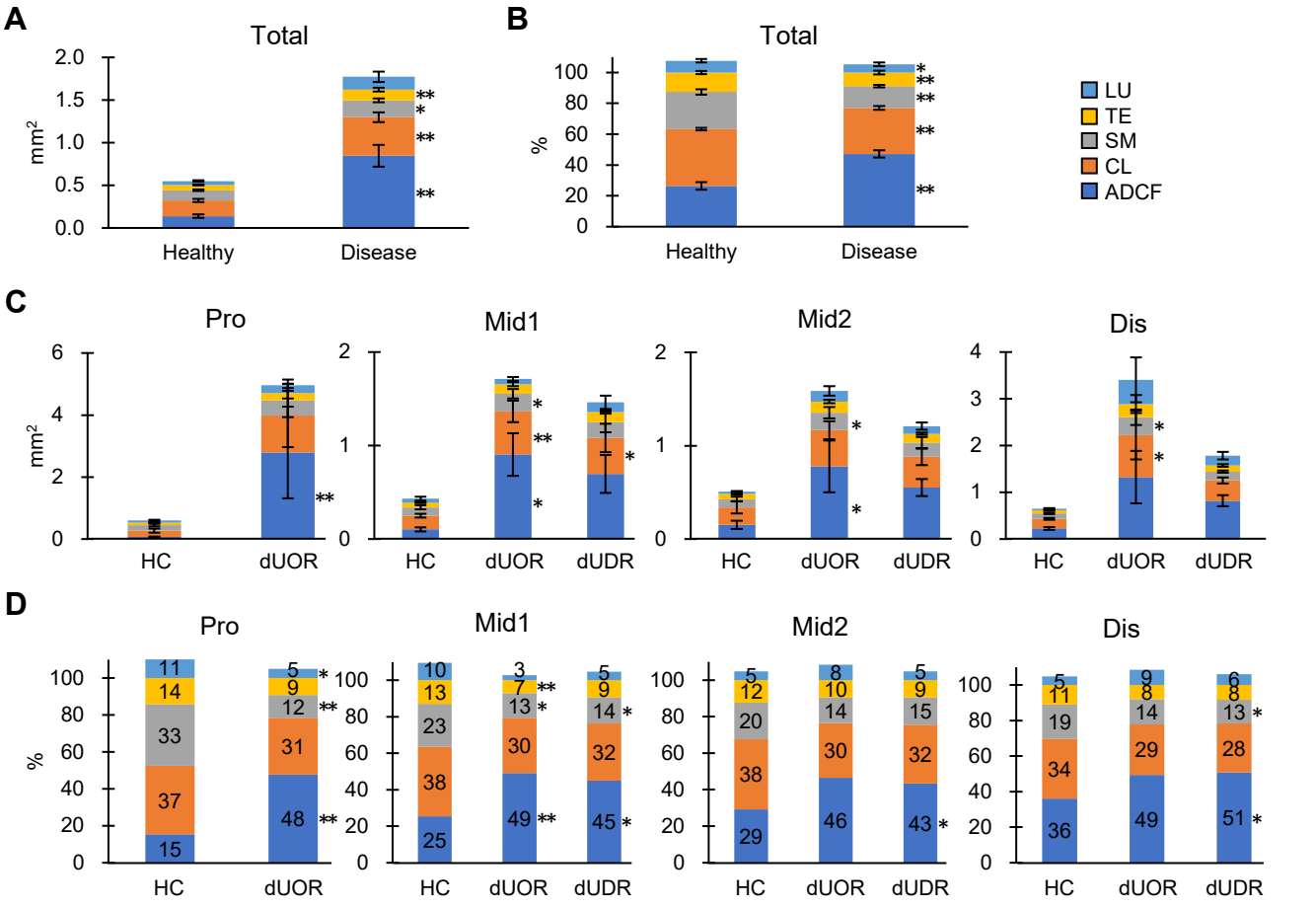
A
Total
mm²
2.0
1.5
1.0
0.5
0.0
Healthy
Disease
B
Total
%
100
80
60
40
20
0
Healthy
Disease
LU
TE
SM
CL
ADCF
C
Pro
Mid1
Mid2
Dis
mm²
HC
dUOR
dUDR
D
Pro
Mid1
Mid2
Dis
%
HC
dUOR
dUDR

Figure 6

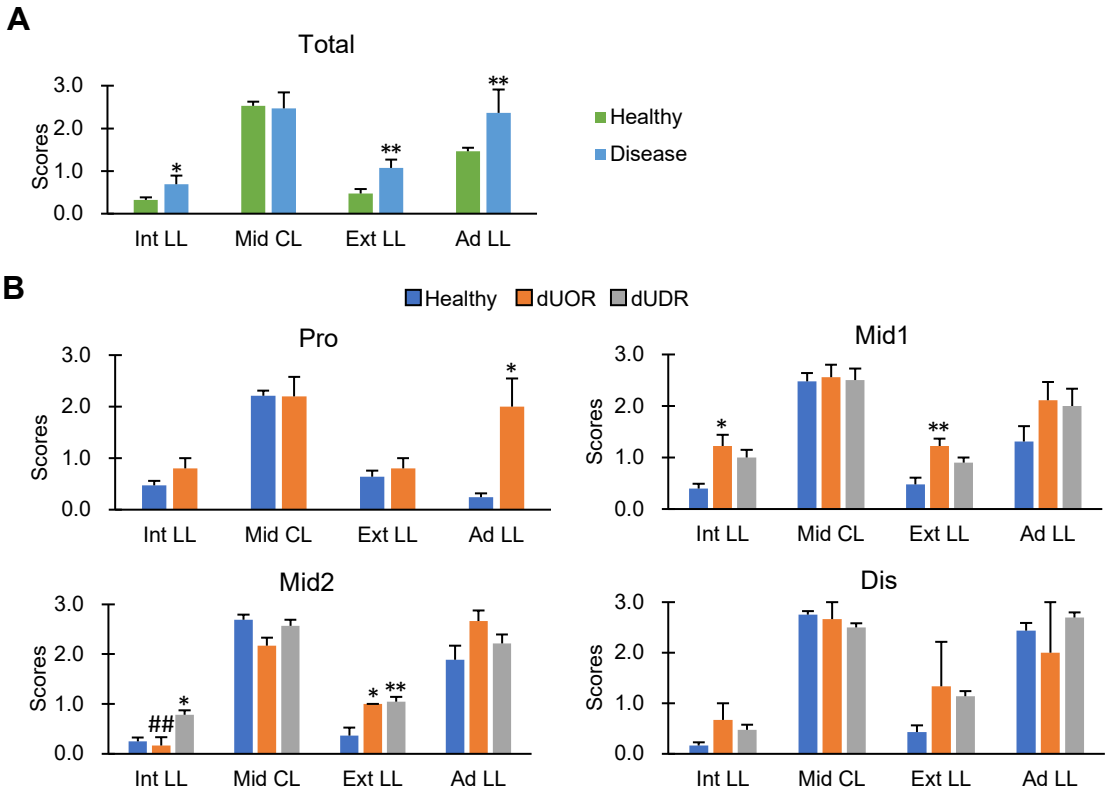
A
Total
Scores
3.0
2.0
1.0
0.0
Int LL
Mid CL
Ext LL
Ad LL
Healthy
Disease
B
Healthy
dUOR
dUDR
Pro
Mid1
Mid2
Dis
##

Figure 7

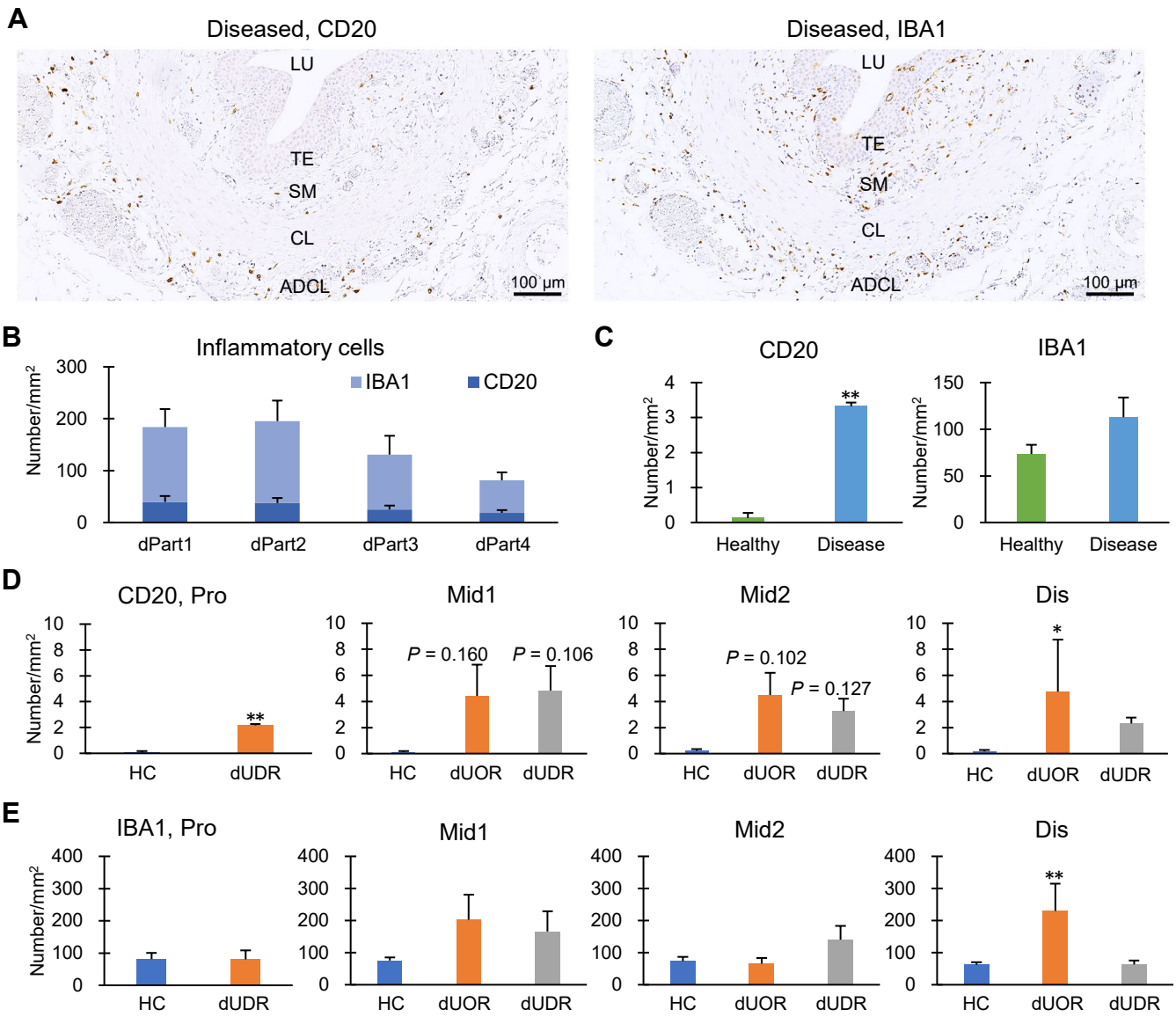
A
Diseased, CD20
LU
TE
SM
CL
ADCL
100 μm
Diseased, IBA1
LU
TE
SM
CL
ADCL
100 μm
B
Inflammatory cells
IBA1
CD20
Number/mm2
300
200
100
0
dPart1
dPart2
dPart3
dPart4
C
CD20
Number/mm2
4
3
2
1
0
**
Healthy
Disease
IBA1
Number/mm2
150
100
50
0
Healthy
Disease
D
CD20, Pro
Number/mm2
10
8
6
4
2
0
**
HC
dUDR
Mid1
P = 0.160
P = 0.106
HC
dUOR
dUDR
Mid2
P = 0.102
P = 0.127
HC
dUOR
dUDR
Dis
*
HC
dUOR
dUDR
E
IBA1, Pro
Number/mm2
400
300
200
100
0
HC
dUDR
Mid1
HC
dUOR
dUDR
Mid2
HC
dUOR
dUDR
Dis
**
HC
dUOR
dUDR

Figure 8

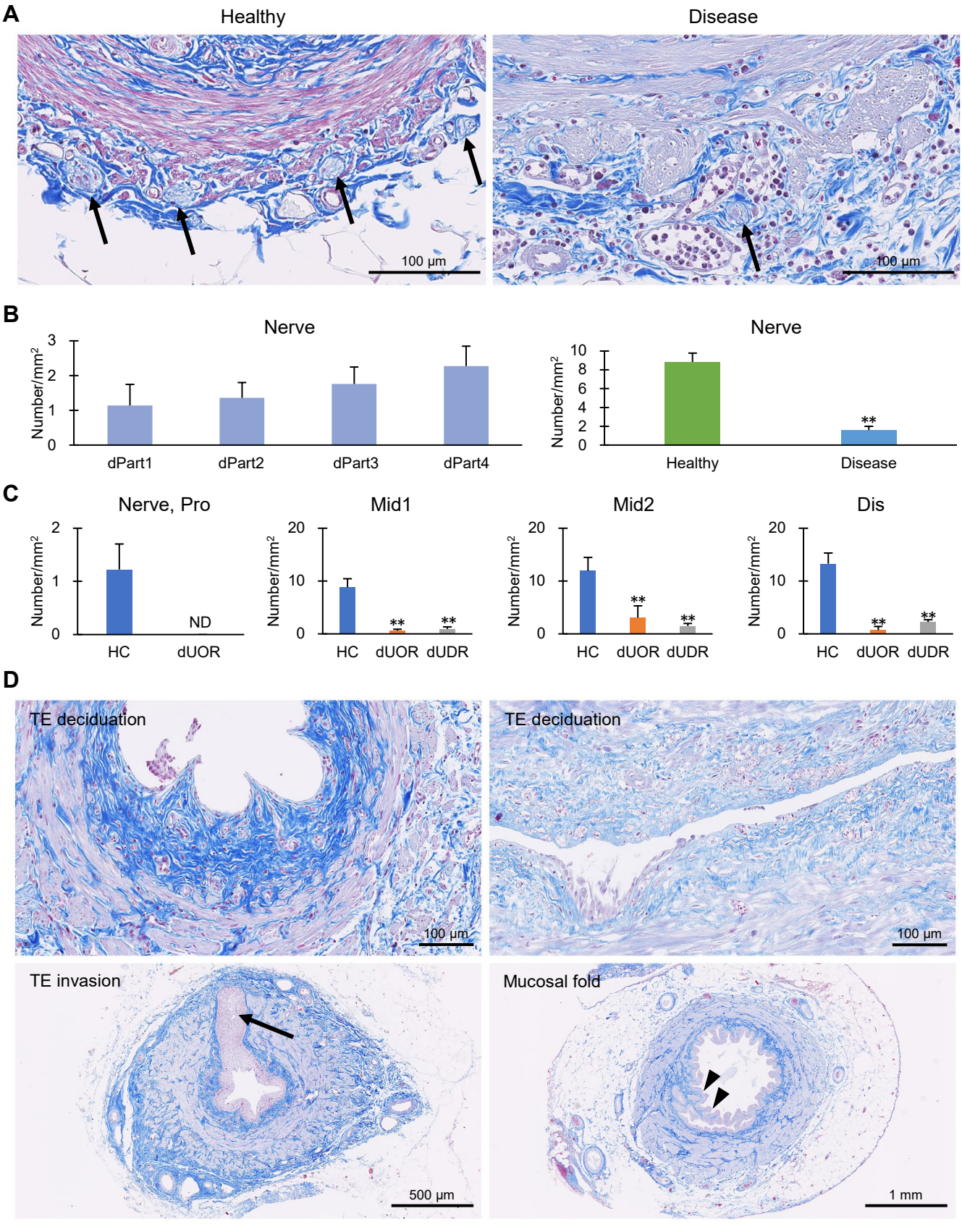
A
Healthy
Disease
100 μm
100 μm
B
Nerve
Number/mm2
dPart1
dPart2
dPart3
dPart4
Nerve
Number/mm2
**
Healthy
Disease
C
Nerve, Pro
Number/mm2
ND
HC
dUOR
Mid1
Number/mm2
**
**
HC
dUOR
dUDR
Mid2
Number/mm2
**
**
HC
dUOR
dUDR
Dis
Number/mm2
**
**
HC
dUOR
dUDR
D
TE deciduation
100 μm
TE deciduation
100 μm
TE invasion
500 μm
Mucosal fold
1 mm